

# Near real-time assimilation in IRI of auroral peak E-region density and equatorward boundary

Yongliang Zhang<sup>a,\*</sup>, Larry J. Paxton<sup>a</sup>, Dieter Bilitza<sup>b</sup>, Rick Doe<sup>c</sup>

<sup>a</sup> *The Johns Hopkins University Applied Physics Laboratory, 11100 Johns Hopkins Road, Laurel, MD 20723, USA*

<sup>b</sup> *George Mason University, 4400 University Drive, Fairfax, VA 22030, USA*

<sup>c</sup> *SRI International, 333 Ravenswood Avenue, Menlo Park, CA 94025, USA*

Received 10 September 2009; received in revised form 11 June 2010; accepted 15 June 2010

## Abstract

The paper describes the method and initial results of assimilating the auroral peak E-region density ( $NmE$ ) and the auroral equatorward boundary (EB) into the International Reference Ionosphere (IRI). The  $NmE$  and EB are obtained using a FUV based auroral model or FUV measurements in near real-time. Initial results show that the auroral  $NmE$  is often significantly larger than the  $NmE$  due to the solar EUV. This indicates the importance of including the contribution of precipitating electrons in IRI. The global equatorial boundary helps to improve the specification of the sub-auroral ionosphere trough in IRI. An IDL software package has been developed to interactively display the IRI parameters with assimilated  $NmE$  and EB. It can serve as an operational tool for space weather monitoring.

© 2010 COSPAR. Published by Elsevier Ltd. All rights reserved.

**Keywords:** IRI; Ionosphere; Auroral peak E-region density; Auroral equatorward boundary

## 1. Introduction

The International Reference Ionosphere (IRI) is a widely used empirical model for ionospheric parameters and the de facto international standard for the ionosphere. IRI describes monthly averages of electron and ion densities and temperatures in the ionospheric altitude range from about 50 km to 1500 km. The development of the model was initiated in the late sixties by the international scientific unions in charge of ionospheric physics, the International Union of Radio Science (URSI) and the Committee on Space Research (COSPAR). Since then the model has steadily evolved from reference tables for specific times and locations to a global model that describes the variation of the ionospheric plasma in space and time. By charter IRI is an empirical model being based primarily on measure-

ments from ground and space; theoretical considerations are used to establish appropriate mathematical functions to describe the dominant variation patterns and they are also used to fill data gaps. The latest version of the model is IRI-2007 as described by Bilitza and Reinisch (2008). The prime focus of the early development was on the middle latitudes because that is where most of the IRI users were in need of a reliable representation of ionospheric characteristics. Combining data from almost all available ground and space data sources the model has now reached a high level of reliability in the mid-latitude ionosphere as documented in extensive comparisons with newer data and in many successful applications ranging from ionospheric corrections for remote sensing from Earth-observing satellite to background ionosphere for testing tomographic techniques and global navigation satellite system (GNSS) mappings to list just two of the many applications of the model. With mid-latitudes well represented efforts are now directed towards an accurate representation of the low and high latitudes. In both regions the modeling pro-

\* Corresponding author.

E-mail address: [Yongliang.Zhang@jhuapl.edu](mailto:Yongliang.Zhang@jhuapl.edu) (Y. Zhang).

cess is complicated by the multitude of processes and the many characteristic structures observed in these parts of the globe.

At high latitude or auroral regions, energetic electron precipitation enhances ionospheric electron densities. During magnetic storms, the ionospheric density due to the precipitating electrons could be significantly larger than the electron density due to the solar EUV flux at high latitudes. The enhanced electron density leads to an increase of ionospheric conductance which affects the Joule heating and plays a very important role in the magnetosphere–ionosphere (M–I) coupling. The magnetospheric energy input (Joule heating and particle heating) is the major source for disturbance in the ionosphere and thermosphere during magnetic storms (Pröls and Craven, 1998; Zhang et al., 2003, 2004). Specification of the ionosphere condition in the auroral region is urgently needed.

A representation of auroral characteristics in IRI has long been an important issue on the agenda of IRI developers (Bilitza, 1995) and users (Szuszczewicz et al., 1993). As a first step towards this goal a model description of auroral boundaries needs to be included in IRI to specify the location of the auroral oval on the globe and to describe the expansion of the oval with increasing magnetic activity. The first generation of auroral oval representations was based on all sky imager observations, e.g., Holzworth and Meng (1975). Next came a series of models that described the precipitating particle flux distribution in the auroral oval based on satellite in situ particle measurements (Wallis and Budzinski, 1981; Spiro et al., 1982; Hardy et al., 1987; Fuller-Rowell and Evans, 1987). Using appropriate flux threshold values one can deduce auroral boundaries from these flux maps. Szuszczewicz et al. (1993) and Bilitza (1995) compared some of these boundary models with data and with each other and made recommendations regarding their use in IRI, but no clear favorite evolved. The most complete representation of auroral electron fluxes and boundaries can be achieved with FUV imagers like GUVI and SSUSI that simultaneously measure UV intensities in several wavelength bands including N<sub>2</sub> LBHS (140–150 nm) and LBHL (165–180 nm). The model of Zhang and Paxton (2008) is the latest and most advanced of these models and will be the base model for introducing auroral boundaries into IRI. Introduction of the boundaries will also not only allow the inclusion of a realistic auroral E-peak model but also other typical high-latitude features like the sub-auroral trough (Pröls, 2007) and the co-located enhancement in electron temperature (Pröls, 2006a,b).

The current version of IRI (Bilitza, 2001; Bilitza and Reinisch, 2008) does not include the contribution from the particle precipitation (mainly electrons (Hardy et al., 1987)) in the auroral oval. The shortcomings in the specification of the high latitude ionosphere, especially the E-region in the auroral oval, are becoming a significant obstacle in improving our understanding and ability to accurately forecast disturbances in the ionosphere and thermosphere

during magnetic storms. The IRI community also has already recognized the need for auroral oval information (e.g., auroral boundary) in IRI for many years (Bilitza, 1995). The availability of a large volume of optical and particle data sets from recent satellite missions allows near real-time global auroral specification and the development of a new auroral model (Zhang and Paxton, 2008). In this paper, we focus on assimilating auroral products (peak auroral E-region density and equatorward auroral boundary) from global spectrographic FUV auroral measurements or the FUV based auroral model into IRI. The FUV (or GUVI) based empirical auroral model can be driven by Kp or measured equatorward auroral boundary. Inclusion of the FUV auroral model allows flexibility in auroral specification in IRI.

## 2. Auroral data and model

### 2.1. Auroral data

Global FUV spectrograph instruments, such as TIMED/GUVI (Paxton and Meng, 1999; Christensen et al., 2003) and DMS/SSUSI (Paxton et al., 2002), simultaneously measure FUV emissions in a few bands including N<sub>2</sub> LBHS (140–150 nm) and LBHL (165–180 nm) at same locations with a high spatial resolution ( $\sim 7$ – $9$  km at nadir). The simultaneous measurements provide a reliable and unbiased way to retrieve the characteristics (mean energy and energy flux) of precipitating electrons. Techniques have been developed to estimate the above two key auroral electron parameters, mean electron energy ( $E_0$ ) and electron energy flux ( $Q$ ), from the FUV auroral data. Strickland et al. (1983) proposed use of the N<sub>2</sub> LBHS and LBHL emissions to estimate  $E_0$  and  $Q$ . Since the emissions of the LBHS and LBHL originate from the same species, their ratio is nearly independent of compositional changes. The key step in transforming the observed auroral LBHS and LBHL intensities into  $E_0$  and  $Q$  of precipitating electrons is to establish a relationship between the observed intensities and these parameters. We first run the Boltzman Three Constituent (B3C) auroral transport code (Daniell, 1993) for Gaussian-distributed precipitating electrons with a fixed energy flux of 1 erg/(cm<sup>2</sup> s) and mean energies varying from 2 to 20 keV. Neutral atmospheric density profiles were taken from the MSIS86 model at a latitude of 60° (typical auroral latitude) with fixed F10.7 (150) and Ap (1) values. The Atmospheric Ultraviolet Radiance Integrated Code (AURIC) (Strickland et al., 1999) is then used to calculate the atmospheric radiance from the profiles of the volume emission rate generated by B3C. The GUVI  $E_0$  and  $Q$  products have been routinely produced and posted on the GUVI website (<http://guvi.jhuapl.edu>). These products were used to develop a FUV based auroral model that covers the whole Kp range (0–9) (Zhang and Paxton, 2008). The same technique also produces peak auroral E-region density ( $NmE$ ) and its associated height ( $hmE$ ). The SSUSI instrument is nearly identical to GUVI.

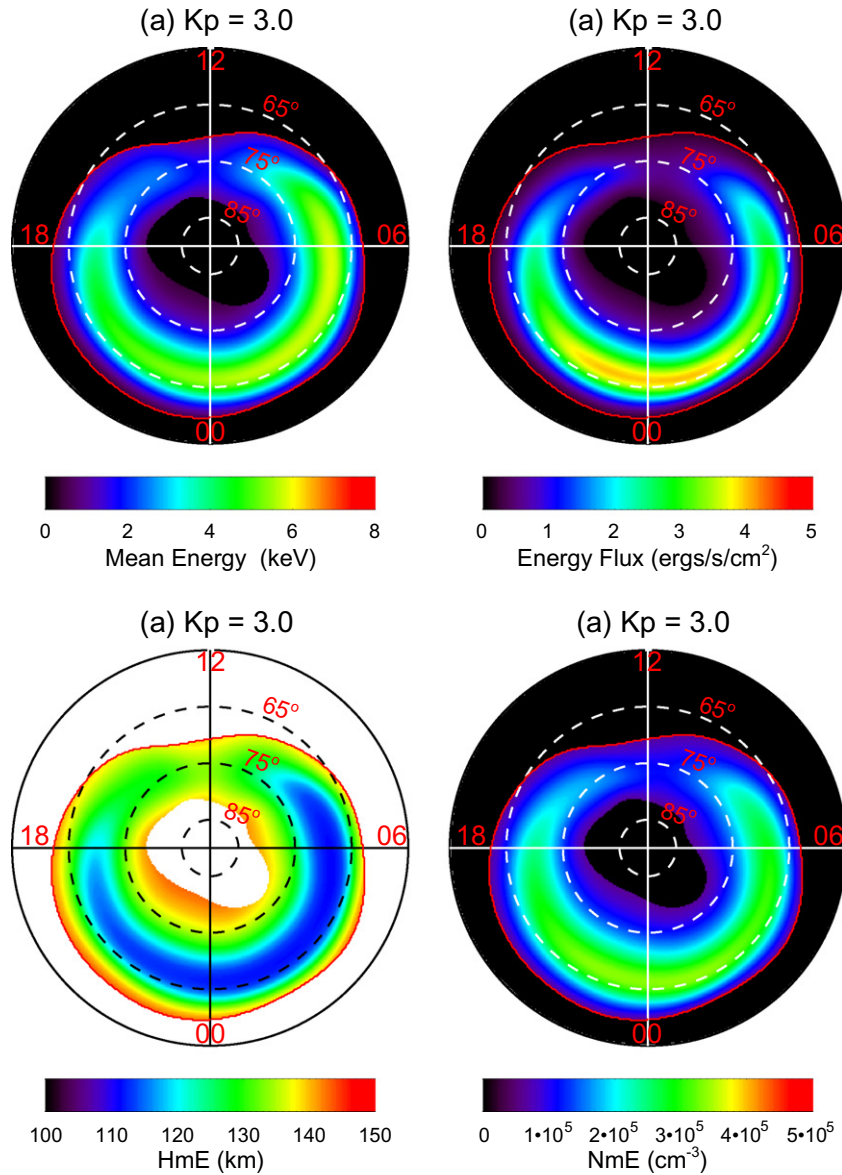


Fig. 1. Results from the GUVI based auroral model: (a) mean energy and (b) energy flux of precipitating electrons, (c) height ( $hmE$ ) of the peak E-region density, and (d)  $NmE$  for  $Kp = 3$ . The plots are in magnetic coordinates (noon at top, mid-night at bottom, dawn at right, dusk at left). The red line shows the auroral equatorward boundary at a fixed flux threshold ( $0.2 \text{ ergs/s/cm}^2$ ). (For interpretation of the references to colour in this figure legend, the reader is referred to the web version of this article.)

GUVI and SSUSI auroral products ( $E_o$ ,  $Q$ ,  $hmE$ ,  $NmE$  and boundary) have been routinely produced in near real-time.

Therefore, it is ideal to use the GUVI and SSUSI auroral products in updating IRI.

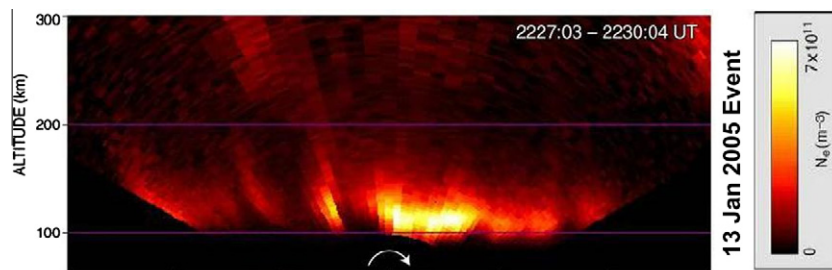


Fig. 2. Auroral ionospheric E-layer electron density profiles obtained from the Sondrestrom Incoherent Scattering Radar between 22:27 and 22:30 UT on January 13, 2005.

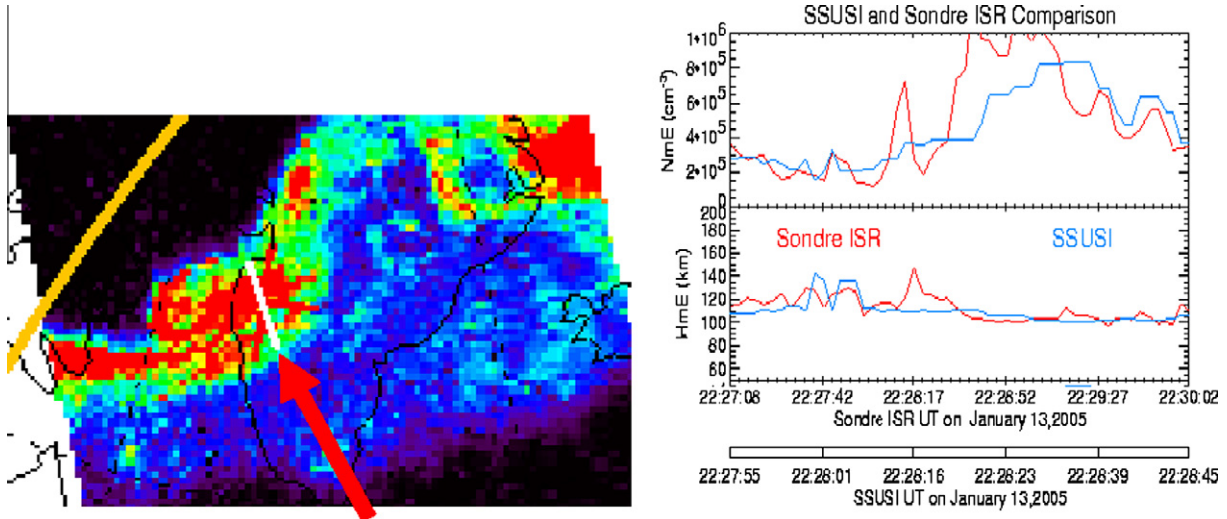


Fig. 3. Left panel: DMSP F16 SSUSI auroral image over Greenland. The white bar over intense aurora (indicated by a solid red arrow) shows the scan track of the Sondrestrom Incoherent Scatter Radar. Right:  $NmE$ ,  $hmE$  along the white bar from SSUSI (blue line) and the radar (red line). (For interpretation of the references to colour in this figure legend, the reader is referred to the web version of this article.)

## 2.2. Auroral model

The FUV based auroral model (Zhang and Paxton, 2008) will also be used in updating IRI. The model is also called GUVI based model as it uses GUVI data. Details of the model description can be found in the reference. Here we show one example of the model outputs for a given

$Kp$ . The outputs (Fig. 1,  $Kp = 3$ ) include  $Eo$ ,  $Q$ ,  $hmE$ ,  $NmE$  and the equatorward boundary in the magnetic latitude (Mlat) and local time (MLT) coordinates. Fig. 1a indicates that the mean energy gradually increases from the dusk side to the night side and the dawn side. The mean energy reaches its minimum on the dayside. On the other hand, the energy flux (Fig. 1b) peaks on the nightside and reaches its minimum on the dayside. These features are consistent with dynamics and the drift path effect of high energy electrons in the central plasmas sheet and day-side cusp electrons with low energy and flux. The flux map also allows us to find the equatorward boundary (see red line in Fig. 1) of the auroral oval at a fixed flux threshold ( $0.2 \text{ ergs/s/cm}^2$ ). The corresponding  $hmE$  and  $NmE$  are shown in Figs. 1c and d. It is clear that the mean energy determines the  $hmE$  (e.g.  $Eo > 6 \text{ keV}$  leads to low  $hmE$  ( $\sim 110 \text{ km}$ )). The  $NmE$  is mostly controlled by the energy flux and thus Fig. 1b and d is similar with each other. Using the FUV based auroral model in IRI provides the benefit of global specification of the aurora in IRI as measurements often have limited spatial coverage. In addition to  $Kp$ , the auroral model can be driven by near real-time measured equatorward auroral boundary.

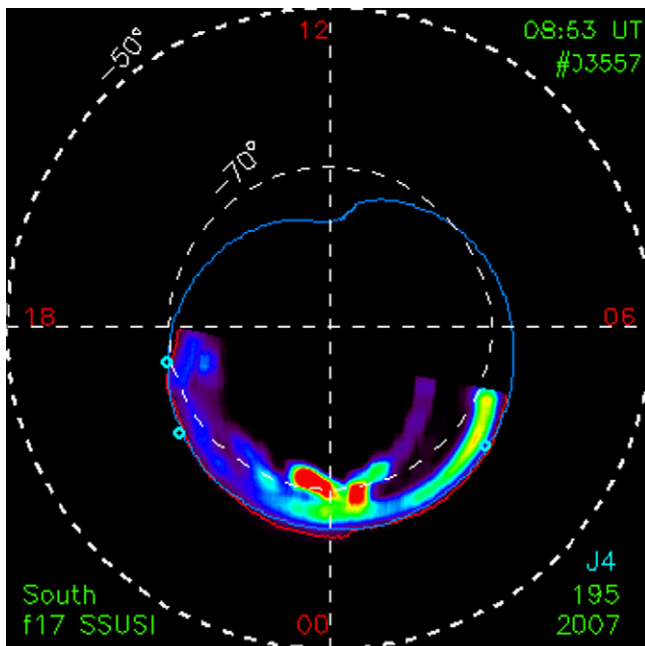


Fig. 4. Individual image of electron energy flux obtained from DMSP F17 SSUSI around 08:53 UT on July 14, 2007 (day of year: 195) in the southern hemisphere. The red line highlights the equatorward boundary. The blue line is the FUV model boundary that has the best fit to the SSUSI boundary. The three small blue circles show the equatorward boundary determined from simultaneous DMSP particle measurements. (For interpretation of the references to colour in this figure legend, the reader is referred to the web version of this article.)

## 3. Validation of auroral $NmE$ , $hmE$ and equatorward boundary

To validate the FUV auroral  $NmE$  and  $hmE$ , the  $NmE$  and  $hmE$  from coincident incoherent scattering radar (ISR) measurements were compared with DMSP F16 SSUSI  $NmE$  and  $hmE$ . Fig. 2 shows one example of the Sondrestrom ISR electron density profiles between 22:27 and 22:30 UT, January 13, 2005. During the period, the ISR scans from South to North (see the white bar in the left panel of Fig. 3 for the scan track). The left panel of Fig. 3 indicates part of the SSUSI auroral image over Greenland. The Son-

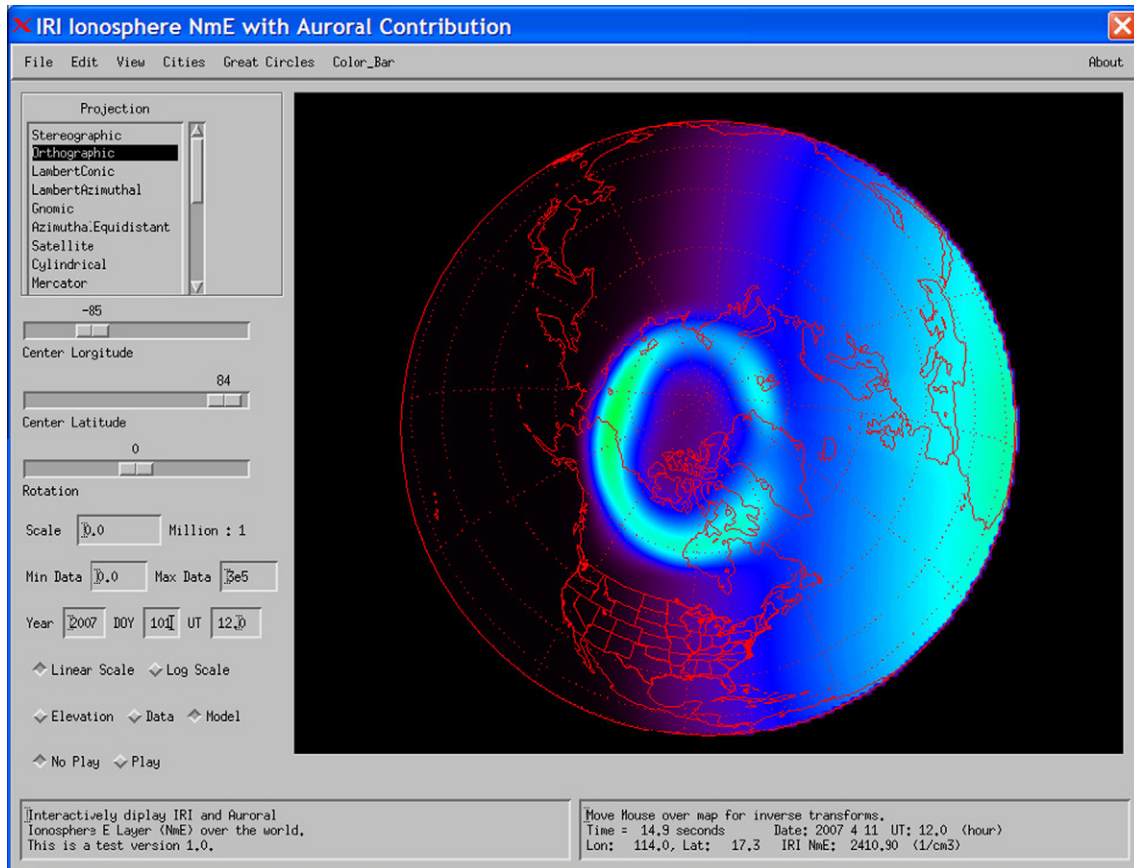


Fig. 5. IRI peak E-region electron density with assimilated auroral  $NmE$  based on the GUVI auroral model. The model was driven by measured Kp index. The display was realized through the IDL interactive software.

drestron ISR was scanning through intense auroras. The right panels in Fig. 3 show the comparison between SSUSI and ISR  $NmE$  and  $hmE$  along the ISR scanning track. Considering the different time and spatial resolutions and techniques used in SSUSI and ISR, and the dynamics of the discrete auroras, the SSUSI  $NmE$  and  $hmE$  agree remarkably well with those from the ISR. This is a typical example among a number SSUSI and ISR coincident events.

The DMSP F16 SSUSI calibration and validation effort has concluded that FUV based  $NmE$  and  $hmE$  values have a fairly good agreement with simultaneous independent incoherent scatter radar measurement during nighttime when the solar contribution is negligible and E-layer ionization is predominantly due to electron precipitation. All these indicate that the FUV based  $NmE$  and  $hmE$  are reliable products that can be used to update IRI in auroral regions.

The location of the auroral oval is also important and needs to be specified as it affects the global ionosphere and thermosphere response to the heating in the auroral region. The oval location is best specified by its equatorward boundaries. There are a number of ways to determine the boundaries. Here, we use a fixed flux threshold ( $0.2 \text{ ergs/s/cm}^2$ ) to find the boundaries as this is the most meaningful way in view of geophysical effectiveness. Fig. 4 shows one example of the electron energy flux map in Mlat-MLT coordinates based on DMSP F17 SSUSI data around 08:53 UT on July

14, 2007 in the southern hemisphere. Note the SSUSI data or swath just covered half of the auroral oval. The red line is the equatorward boundary of the SSUSI swath. It was called swath boundary, and is used to find the global boundary (blue line) by fitting the GUVI model based boundary (see example in Fig. 1) and the swath boundary. The small blue circles show the location of the equatorward boundary based on simultaneous DMSP particle data. It is clear that there is a very good agreement among the swath, global and independent particle boundaries. A statistical study done as part of the SSUSI calibration and validation effort also concluded that the SSUSI equatorward auroral boundary agrees well with the boundary determined from coincident particle measurements for relatively bright auroras with sharp boundaries.

#### 4. Assimilating $NmE$ and auroral boundary in IRI

##### 4.1. Assimilating modeled $NmE$ in IRI

The IRI outputs are usually specified in geographic coordinates. The GUVI auroral model, however, is based on magnetic latitude and local time. The first step is to transform the modeled  $NmE$  and boundary into geographic coordinates. We use AACGM (Altitude Adjusted CGM) (Baker and Wing, 1989) to do the transform by

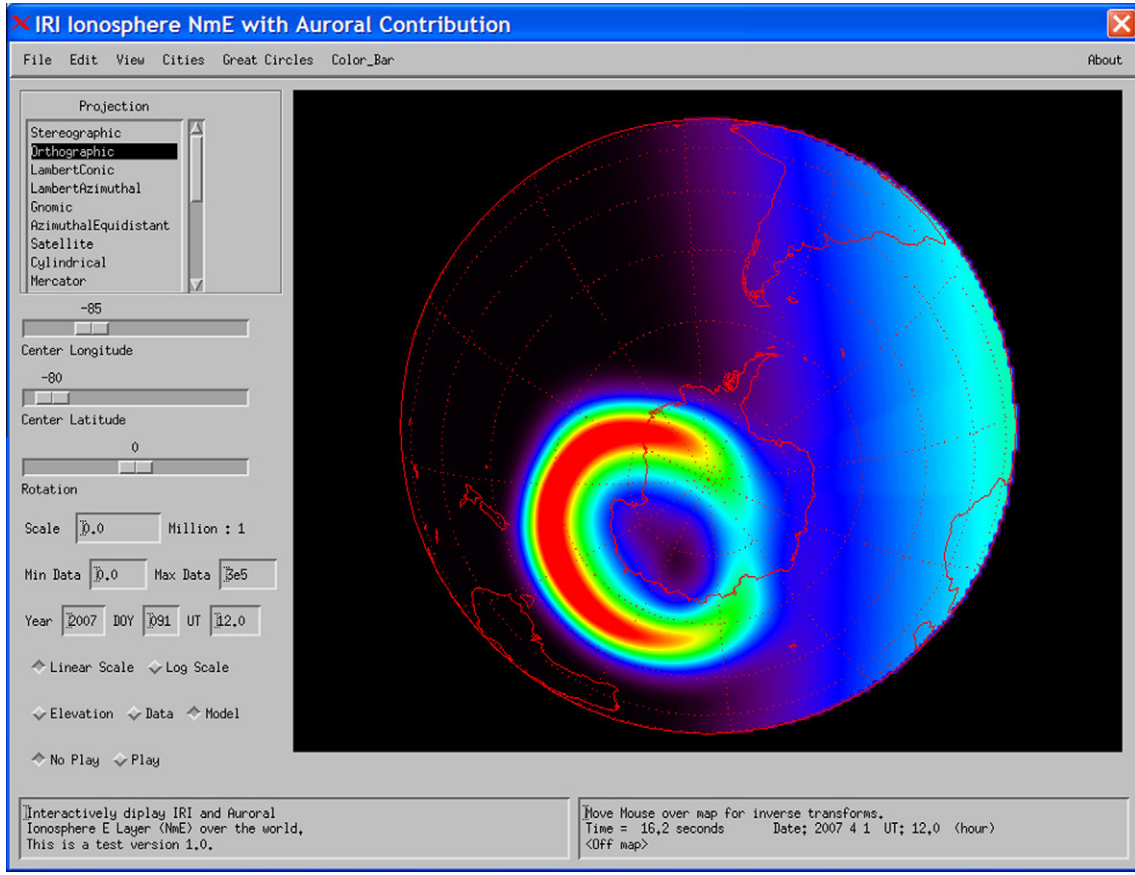


Fig. 6. Similar to Fig. 5 but for different date in the southern hemisphere.

assuming an altitude of 110 km, a typical height of auroral E-region peak density. The second step is to merge the  $NmE$  due to electron precipitation and solar EUV flux. In the auroral ionosphere, the electron density ( $N_e$ ) is determined by the continuity equation (see the Eq. (1)), where  $V_e$  is the electron bulk velocity. The  $P_{ewv}$  and  $P_e$  are the electron production rates due to solar EUV flux and electron precipitation, respectively. The  $\alpha N_e^2$  is the electron loss rate due to ion–electron recombination. In the ionosphere E-region, the strong ion–neutral collision allows to neglect the convection term. We further assume that the ionization process quickly reaches local equilibrium, thus the time variation of  $N_e$  is 0. The electron density can then be determined by Eq. (2)

$$\frac{\partial N_e}{\partial t} + \nabla \cdot (N_e \vec{V}_e) = P_{ewv} + P_e - \alpha N_e^2 \quad (1)$$

$$\alpha N_e^2 = P_{ewv} + P_e \quad (2)$$

Let  $N_e^{ewv}$  represent the electron density due to solar EUV only and  $N_e^e$  due to electron precipitation only. They satisfy following conditions, similar to Eq. (2)

$$\alpha (N_e^{ewv})^2 = P_{ewv} \quad (3)$$

$$\alpha (N_e^e)^2 = P_e \quad (4)$$

Combining Eqs. (2)–(4) gives:

$$N_e = \sqrt{(N_e^{ewv})^2 + (N_e^e)^2} \quad (5)$$

As the ionosphere E-region peak heights due to solar EUV or typical precipitating electrons (a few keV) are roughly around 110 km, the Eq. (5) can be applied to the  $NmE$ . IRI provides solar EUV based  $NmE$  and the auroral model gives electron precipitation based  $NmE$ . Eq. (5) combines them to provide assimilated  $NmE$  (see one example in Fig. 5 in the northern hemisphere). The display in Fig. 5 was created using IDL widgets that call the IRI and the auroral model, assimilate the  $NmE$ , and interactively show the location and associated  $NmE$  value at the computer mouse position. The IDL widgets also allow free rotation and zoom of the earth for either global or local view. In addition to the model  $NmE$ , the near real-time GUVI and SSUSI auroral products have been successfully assimilated to IRI using the IDL software.

Fig. 6 shows another example of model  $NmE$  that was assimilated into IRI for different date and in the southern hemisphere. Both of Figs. 5 and 6 indicate that the  $NmE$  due to precipitating electrons is much larger than the  $NmE$  due to solar EUV radiation at the auroral latitudes. This confirms the importance of including contribution of the precipitating electrons in IRI. The equatorward boundary from the auroral model (see Fig. 1) was not included in Figs. 5 and 6. But the boundary was included with near real-time FUV aurora data (see examples later).

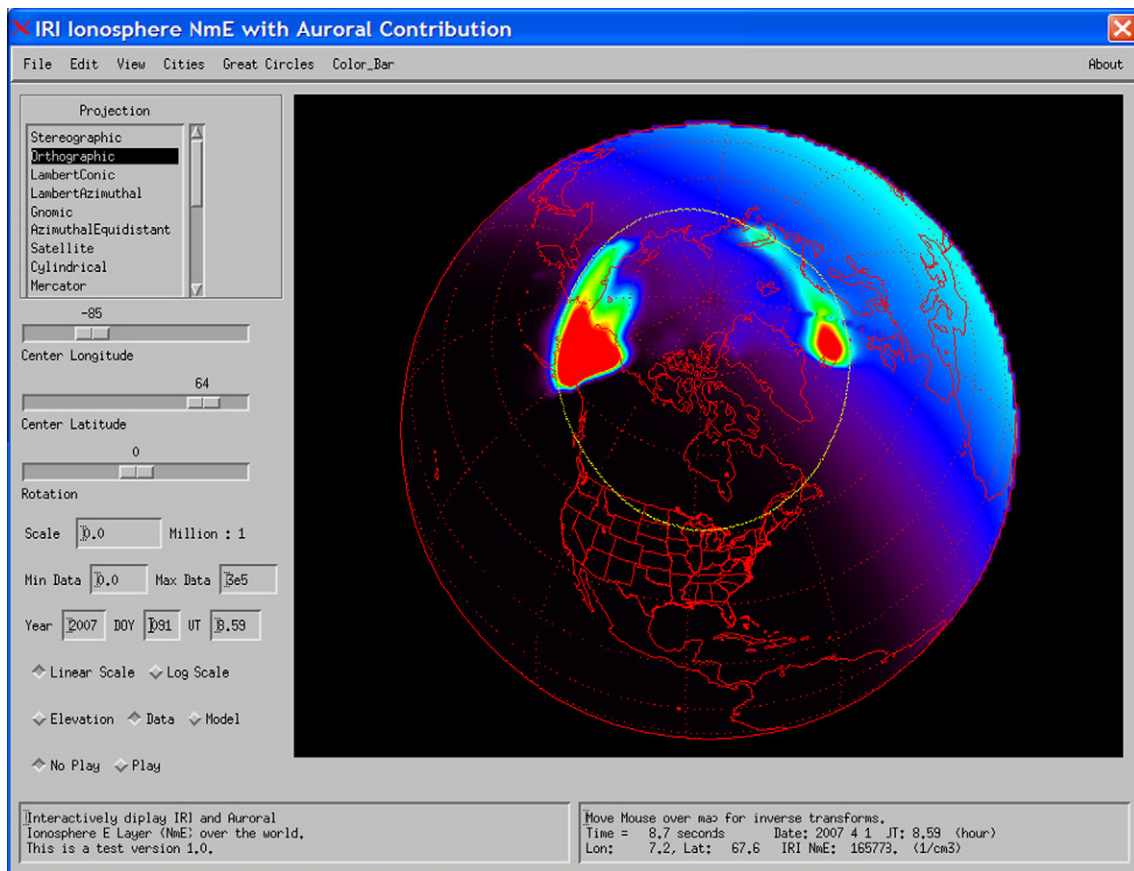


Fig. 7. Near real-time assimilation of SSUSI  $NmE$  into IRI on the northern hemisphere. The yellow line is the fitted global equatorial model boundary. The enhanced  $NmE$  in polar region indicates the swath of SSUSI measurements. (For interpretation of the references to colour in this figure legend, the reader is referred to the web version of this article.)

#### 4.2. Assimilating near real-time measured $NmE$ and boundary in IRI

Using the same method described in Section 4.1, the near real-time or historical auroral products ( $NmE$  and boundary) from SSUSI and GUVI has been assimilated into IRI. Fig. 7 shows one example of IRI with assimilated SSUSI  $NmE$  and global boundary (yellow line). Despite of limited spatial coverage of SSUSI data, the SSUSI  $NmE$  provide an indicator of magnitude of auroral  $NmE$  as well as the global auroral oval location through the boundary. The example in Fig. 7 also demonstrates that the FUV spectrographic imaging technique allows SSUSI and GUVI to detect auroral emissions and generate auroral products under both nighttime and sunlit conditions. Fig. 8 shows another example at different time on the southern hemisphere. Again, these examples indicate that the auroral  $NmE$  can be much larger than the solar EUV  $NmE$  at high latitudes.

### 5. Discussion

The advanced FUV spectrographic imaging technique used in SSUSI and GUVI provides accurate atmospheric emission intensities simultaneously from same locations

over different wavelength bands. This technique eliminates the errors due to out of band contribution, non-simultaneous measurements and different fields of view in traditional filter based FUV imagers. With the B3C and AURIC modeling tools, the SSUSI and GUVI data provide unbiased estimation of the characteristics of precipitating electrons and associated ionospheric parameters ( $NmE$ ,  $hmE$  and boundary). The validation of the auroral ionospheric products demonstrated the value of the SSUSI and GUVI auroral products. One important feature from the  $NmE$  assimilation is that the auroral  $NmE$  is significantly larger than the  $NmE$  due to solar EUV. This confirms the urgent need to include auroral contribution in IRI as accurate specification of E-region electron density is very important for a better estimation and understanding of storm time Joule heating, the major driver of the ionosphere and thermosphere space weather.

The above results support the early simulation conclusions. Comparison between TGCM runs (Roble and Ridley, 1987) with and without auroral precipitation shows that relatively soft particles ( $\sim 1\text{--}2$  keV) provide sufficient ionization in the lower ionosphere to be competitive with solar photo-ionization and can alter the dynamics in the lower thermosphere in the summer hemisphere. In the winter hemisphere, particle precipitation has a much larger

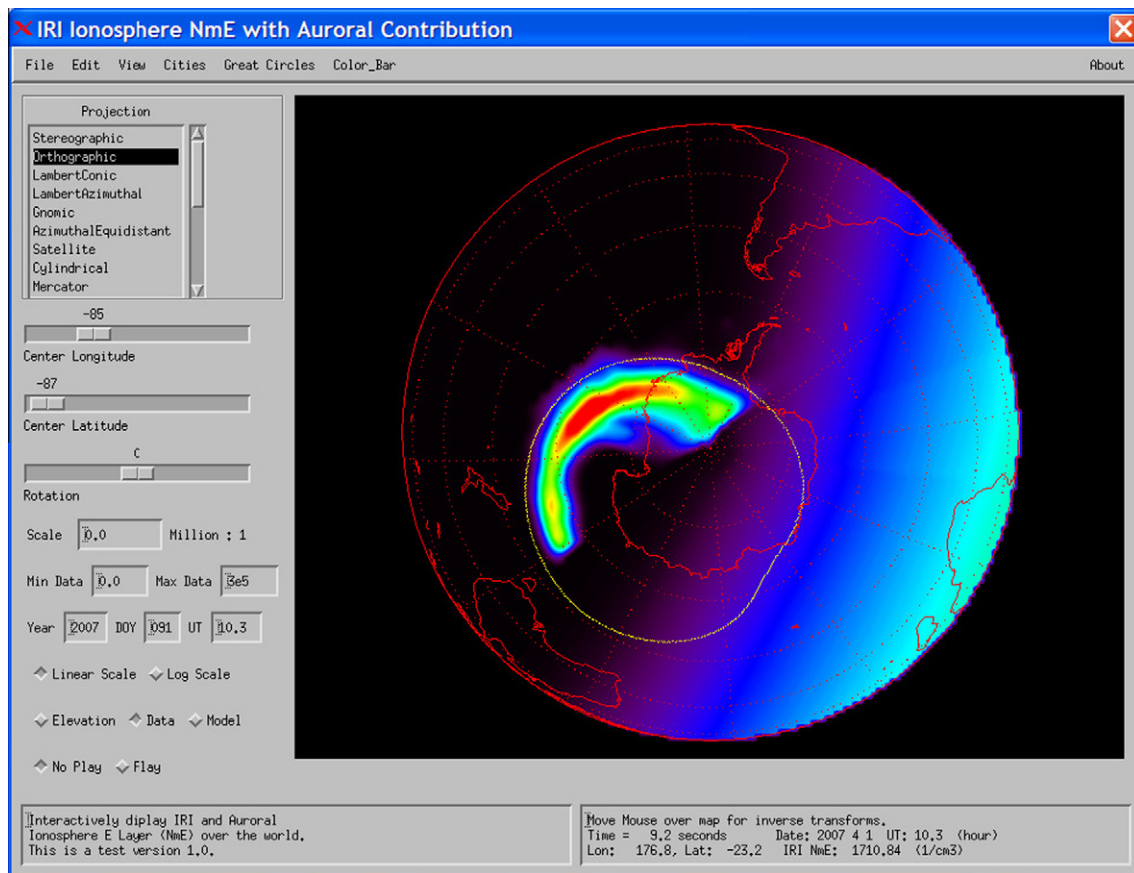


Fig. 8. Similar to Fig. 7 but for different time and southern hemisphere.

influence on the dynamical structure of both the upper and lower thermosphere. Roble and Ridley (1987) found that at the F-region heights ( $\sim 300$  km) both the polar cap temperature and wind velocity increased due to auroral precipitation. The dusk cell convection velocities are enhanced and reach a maximum velocity of 70 m/s. Enhanced Joule heating produces a temperature increase of about 50 K in the polar cap. In addition, Roble and Ridley (1987) found that auroral particle precipitation provides sufficient ionization in the lower thermosphere to alter the circumpolar circulation. Such an effect is more significant in the winter hemisphere. These indicate that the IRI with assimilated auroral  $NmE$  could also be useful to specify polar ionosphere conditions in global ionosphere, thermosphere, or magnetosphere simulations.

In addition to the  $NmE$ , location of the enhanced ionization or auroral oval is also important. It is expected that the ionosphere and thermosphere will have different responses if the enhanced  $NmE$  with the same magnitude is located at different latitudes. Inclusion of the equatorward auroral boundary in IRI (as shown in Figs. 7 and 8) will also improve the specification of auroral ionosphere in IRI and help all applications that use IRI in high latitudes.

The interactive IDL display tool demonstrates that the  $NmE$  and auroral boundary assimilation in IRI can be done in near real-time. Furthermore, when a predicted

$Kp$  is available, the FUV auroral model could be used to forecast the auroral products.

## 6. Summary and future work

The global IRI community has been continuously working on improving the International Reference Ionosphere. Assimilation auroral  $NmE$  and equatorward boundary in IRI is part of the improvement efforts. The FUV auroral data and products from SSUSI and GUVI as well as the FUV based auroral model provide unique data sources and tool to update the IRI in near real-time. The interactive IDL display package provides a useful way to monitor the polar and global E-region peak density in near real-time. It can also be used as space weather operation tool.

The next step is to assimilate auroral E-region density profiles in IRI. This will remove the requirement that the  $hmE$  due to precipitating electron is around 110 km, the IRI  $hmE$ . We also plan to translate the FUV auroral model (currently in IDL) to FORTRAN and make it a part of future IRI.

## Acknowledgements

The authors thank the reviewers for their helpful comments. This work was supported by NSF Grant ATM-

0819771. The equatorward auroral oval boundaries from the DMSP particle data were provided by Dan Ober and Gordon Wilson.

## References

- Baker, K.B., Wing, S. A new magnetic coordinate system for conjugate studies at high latitudes. *J. Geophys. Res.* 94, 9134–9139, 1989.
- Bilitza, D. Including auroral oval boundaries in the IRI model. *Adv. Space Res.* 16 (1), 13–16, 1995.
- Bilitza, D. International reference ionosphere 2000. *Radio Sci.* 36, 261–275, 2001.
- Bilitza, D., Reinisch, B.W. International reference ionosphere 2007: improvements and new parameters. *Adv. Space Res.* 42, 599–610, doi:10.1016/j.asr.2007.07.048, 2008.
- Christensen, A.B., Paxton, L.J., Avery, A., Craven, J., Crowley, G., Jumm, D.C., Kil, H., Meier, R.R., Meng, C.-I., Morrison, D., Ogorzalek, B.S., Straus, P., Strickland, D.J., Swenson, R.M., Walterscheid, R.L., Wolven, B., Zhang, Y. Initial observations with the Global Ultraviolet Imager (GUVI) in the NASA TIMED satellite mission. *J. Geophys. Res.* 108 (A12), 1451–1466, doi:10.1029/2003JA009918, 2003.
- Daniell Jr., R.E. Modeling of optical signatures of electron spectra in the ionospheric heating experiments, in: *Proceedings and Program for the Seventh International Ionospheric Effects Symposium, SRI-Int, Arlington, VA, USA, 1993*, p. 6B/5/1, 1993.
- Fuller-Rowell, T.J., Evans, D.S. Height-integrated Pedersen and Hall conductivity patterns inferred from the TIROS-NOAA satellite data. *J. Geophys. Res.* 92, 7606–7618, 1987.
- Hardy, D.A., Gussenhoven, M.S., Raistrick, R., McNeil, W.J. Statistical and functional representations of the pattern of auroral energy flux, number flux, and conductivity. *J. Geophys. Res.* 92, 12275–12294, 1987.
- Holzworth, R.H., Meng, C.-I. Mathematical representation of the auroral oval. *Geophys. Res. Lett.* 2, 377–380, 1975.
- Paxton, L.J., Meng, C.-I. Auroral imaging and space-based optical remote sensing. *J. Hopkins APL Tech. D.* 20, 556–569, 1999.
- Paxton, Larry J., Morrison, Daniel, Zhang, Yongliang, Kil, Hyosub, Wolven, Brian, Ogorzalek, Bernard S., Humm, David, Meng, Ching-I. Validation of remote sensing products produced by the special sensor ultraviolet scanning imager (SSUSI) – a far-UV imaging spectrograph on DMSP F16, in: *Optical Spectroscopy Techniques, Remote Sensing, and Instrumentation for Atmospheric and Space Research IV*, vol. 4485, pp. 338–348, 2002.
- Prölss, G.W., Craven, J.J. Perturbations of the FUV dayglow and ionospheric storm effects. *Adv. Space Sci.* 22, 129–132, 1998.
- Prölss, G.W. Subauroral electron temperature enhancement in the nighttime ionosphere. *Ann. Geophys.* 24, 1871–1885, 2006a.
- Prölss, G.W. Electron temperature enhancement beneath the magnetospheric cusp. *J. Geophys. Res.* 111, A07304, 1–13, doi:10.1029/2006JA011618, 2006b.
- Prölss, G.W. The equatorward wall of the subauroral trough in the afternoon/evening sector. *Ann. Geophys.* 25, 645–659, 2007.
- Roble, R.G., Ridley, E.C. An auroral model for the NCAR thermospheric general circulation model (TGCM). *Ann. Geophys.* 5A, 369–382, 1987.
- Spiro, R.W., Reif, P.H., Mather, L.J. Precipitating electron energy flux and auroral zone conductances: an empirical model. *J. Geophys. Res.* 87, 8215–8227, 1982.
- Strickland, D.J., Jasperse, J.R., Whalen, J.A. Dependence of auroral FUV emissions on the incident electron spectrum and neutral atmosphere. *J. Geophys. Res.* 88, 8051–8062, 1983.
- Strickland, D.J., Bishop, J., Evans, J.S., Majeed, T., Shen, P.M., Cox, R.J., Link, R., Huffman, R.E. Atmospheric ultraviolet radiance integrated code (AURIC): theory, software architecture, inputs, and selected results. *J. Quant. Spectrosc. Radiat. Transfer* 62, 689–742, 1999.
- Szuszczewicz, E.P., Wilkinson, P., Swider, W., Pulinets, S., Abdu, M.A., Roelof, E., Fuller-rowell, T., Evans, D.S., Bateman, T., Blanchard, P., Gustafsson, G., Hanbaba, R., Joselyn, J., Kikuchi, T., Leitinger, R., Lester, M., Reddy, B., Ruohoniemi, M., Sands, M., Sobral, J., Walker, G.O., Wickwar, V. Measurements and empirical model comparisons of F-region characteristics and auroral oval boundaries during the solstitial SUNDIAL campaign of 1987. *Ann. Geophys.* 11, 601–613, 1993.
- Wallis, D.D., Budzinski, E.E. Empirical models of height-integrated conductivities. *J. Geophys. Res.* 86, 125–137, 1981.
- Zhang, Y., Paxton, L.J., Kil, H., Meng, C.-I., Mende, S.B., Frey, H.U., Immel, T.J. Negative ionospheric storms seen by the IMAGE FUV instrument. *J. Geophys. Res.* 108, 1343–1353, doi:10.1029/2002JA009797, 2003.
- Zhang, Y., Paxton, L.J., Morrison, D., Wolven, B., Kil, H., Meng, C.-I., Mende, S.B., Immel, T.J. O/N<sub>2</sub> changes during 1–4 October 2002 storms: IMAGE SI-13 and TIMED/GUVI observations. *J. Geophys. Res.* 109, A10308, 1–16, doi:10.1029/2004JA010441, 2004.
- Zhang, Y., Paxton, L.J. An empirical Kp-dependent global auroral model based on TIMED/GUVI data. *J. Atmos. Solar – Terr. Phys.* 70, 1231–1242, 2008.